Journal of Science and Transport Technology
Journal homepage: https://jstt.vn/index.php/en

UNIVERSITY OF TRANSPORT TECHNOLOGY

A Process-Based Framework for Early-Age Volumetric Stability in Foamed Controlled Low-Strength Material

Trong-Phuoc Huynh[1], Khanh Duy Le[2], Trung-Hieu Le[3], Tri Ho Minh Le[2,*]

[1]Faculty of Civil Engineering, College of Engineering, Can Tho University, Campus II, 3/2 Street, Ninh Kieu Ward, Can Tho City 94000, Vietnam

[2]Faculty of Civil Engineering, Nguyen Tat Thanh University, No. 300A, Nguyen Tat Thanh Street, Xom Chieu Ward, Ho Chi Minh City, Vietnam

[3]AMS4 Research Group (Advanced Materials and Smart Structure for Sustainable System), University of Transport Technology, 54 Trieu Khuc Street, Thanh Liet Ward, Hanoi, Vietnam

Article info
Type of article:
Original research paper

DOI:
https://doi.org/10.58845/jstt.utt.2026.en.6.4.108-129

[*]**Corresponding author:**
Email address:
lhmtri@ntt.edu.vn

Received: 23/02/2026
Received in Revised Form: 17/05/2026
Accepted: 30/05/2026

Abstract: Early-age volumetric instability severely constrains the reliability of foamed controlled low-strength material (CLSM) when high foam fractions are required for lightweight backfilling. While prior studies emphasize compositional modification, this work demonstrates that geometric stability is primarily governed by shear history during mixing. A process-based framework was established to decouple process control from material stabilization in dredged-soil-based CLSM. Foam content (10–30%), mixing sequence (K, U1, U2), and rotational speed (30–120 rpm) were first evaluated to quantify shear-induced instability. As foam content increased from 10% to 30%, ΔV_Final increased from 1.47% to 19.82%, indicating a pronounced stability threshold beyond 25% foam. Under identical foam content, the staged-water method (U2) at 60 rpm reduced ΔV_Final to 5.91%, approximately 53–55% lower than the dry-mix condition, confirming the dominant role of mixing sequence and controlled shear. Material modifications acted as secondary stabilizers. Surfactant at 0.15% reduced ΔV_Final to 4.21% through interfacial reinforcement. FA replacement at 25% improved rheological cohesion, lowering ΔV_Final to 4.56%. Coconut fiber showed criterion-dependent optima: 0.30% minimized ΔV_Final to 4.89%, whereas 0.20% yielded the highest 28-day compressive strength within the fiber series (1.62 MPa). The integrated SFC configuration achieved ΔV_Final of 2.78% and 28-day compressive strength of 1.62 MPa, compared with 1.42 MPa for the baseline. The findings establish that early-age stability in foamed CLSM is process-dominant, with material strategies providing hierarchical reinforcement across interfacial, rheological, and structural scales. The proposed process–material integration framework establishes shear history as a governing design variable in foamed CLSM and provides a reproducible pathway for balancing lightweight performance with geometric stability in soft-ground backfilling applications.

Keywords: Foamed CLSM; early-age volumetric stability; mixing sequence; shear regime; fly ash; coconut fiber.

1. Introduction

Controlled low-strength material (CLSM) has progressively evolved from a utility trench backfill material into a broader class of flowable cementitious systems designed for controlled structural performance. In soft-ground environments, particularly those characterized by high groundwater levels and compressible alluvial deposits, the density of the backfill material becomes a decisive design parameter. Foamed CLSM, in which preformed air bubbles are intentionally introduced into a cementitious slurry, provides a rational means of reducing self-weight while maintaining flowability and sufficient load-bearing capacity. The engineering premise is straightforward: by replacing part of the solid matrix with stabilized air voids, vertical stress transfer to weak subsoil can be minimized. However, the stability of these intentionally entrained voids remains a critical challenge.

The influence of air content on mechanical behavior has been widely documented. Previous studies have established that increasing porosity leads to predictable reductions in compressive strength and elastic modulus, primarily due to the reduced effective load-bearing cross-section and stress concentration around voids [1]. While these relationships are relatively well understood for hardened-state performance, the mechanisms governing pore stability during the fresh and setting stages are less comprehensively addressed. In foamed systems, the void network is not static; it evolves dynamically from the moment of mixing until structural setting. Bubble rupture, coalescence, drainage-induced thinning of liquid films, and gravitational segregation collectively determine whether the intended pore architecture is preserved.

Research on foaming agents has provided important insights into bubble formation and stabilization. Protein-based foaming agents and synthetic surfactants have been compared in terms of bubble size distribution, film elasticity, and resistance to coalescence [2–4]. These studies emphasize the chemical stabilization of the air–liquid interface, highlighting the role of surface tension reduction and film strengthening in prolonging bubble survival. Nevertheless, such stabilization mechanisms are typically evaluated under relatively controlled rheological conditions, often without explicitly accounting for the shear history imposed during practical mixing operations. As a result, foam stability is frequently interpreted as an intrinsic property of the foaming agent, whereas in reality it is strongly influenced by mechanical disturbances prior to matrix stiffening.

Parallel efforts have explored fiber reinforcement as a means of improving the structural performance of lightweight cementitious materials. The inclusion of micro- or short fibers has been shown to enhance crack resistance, increase post-cracking ductility, and improve load transfer within porous matrices [5]. In aerated systems, fibers can also influence the continuity of the solid phase, potentially restraining local deformation and redistributing stress concentrations. However, most investigations have focused on hardened-state mechanical improvements rather than early-age volumetric stability. The potential role of fibers in constraining bubble migration or mitigating settlement prior to final set has not been systematically examined in the context of foamed CLSM.

Rheology-centered approaches have gained increasing attention in recent years, particularly in applications such as 3D printing and flowable backfills [6–10]. These studies demonstrate that viscosity modifiers, thixotropic agents, and particle packing optimization can significantly influence buildability and resistance to volumetric instability. From a mechanistic perspective, rheological parameters govern the balance between gravitational forces acting on bubbles and the viscous resistance of the surrounding matrix. A sufficiently cohesive paste can retard drainage and delay coalescence, thereby enhancing volumetric stability. Yet, while rheology is acknowledged as important, the explicit interaction between mixing sequence, shear intensity, and subsequent structural locking is rarely isolated as a design variable.

The incorporation of supplementary cementitious materials, particularly fly ash (FA), has also been extensively studied in lightweight and foamed systems [8, 9, 11]. FA modifies particle packing density, reduces water demand, and influences hydration kinetics. Its spherical morphology may enhance flowability, while its pozzolanic reactivity contributes to later-age strength development. In lightweight matrices, FA can refine pore connectivity and improve matrix cohesion, potentially reducing drainage-driven settlement. However, most investigations consider FA primarily from a mechanical or durability perspective, rather than as a stabilizing agent in the early-age evolution of foamed pore structures.

Water management strategies have likewise been examined in relation to volumetric changes. The use of superabsorbent polymers and internal curing agents has been proposed to mitigate shrinkage and regulate moisture redistribution [12]. These approaches highlight the importance of internal water transport in controlling deformation. Nonetheless, shrinkage phenomena addressed in such studies often occur after setting, whereas the rapid volumetric loss observed in foamed CLSM prior to initial set is governed by fluid mechanics and bubble stability rather than autogenous shrinkage mechanisms.

Domestic research efforts have advanced the development of lightweight cementitious materials and aerated concretes, including adaptations for locally available resources [13–15]. These studies demonstrate the feasibility of producing low-density systems suitable for regional applications. However, early-age volumetric instability is commonly reported as an observed limitation rather than dissected as a mechanistic problem. In particular, the integration of dredged soil—a material characterized by fine particle size distribution and variable water demand—introduces additional complexity in terms of rheology and drainage sensitivity.

A critical synthesis of the literature, therefore, reveals two overarching deficiencies. First, foam stability has predominantly been treated as a chemical or compositional issue, with limited systematic investigation of mixing sequence and shear regime as independent design parameters. In high-air-content systems, bubble survival is inherently linked to mechanical history. The order of water addition, the timing of foam incorporation, and the magnitude of applied shear determine whether bubbles are encapsulated within a cohesive matrix or subjected to destructive coalescence prior to structural locking. Without isolating these process variables, it is difficult to distinguish between material-induced and process-induced volumetric instability. Second, volumetric loss is rarely monitored in a time-resolved manner across the transition from fresh state to final set. Deformation occurring before the initial set is governed primarily by fluid dynamics, drainage, and bubble migration, whereas deformation after the initial set reflects the evolving stiffness of the cementitious skeleton. Treating volumetric loss as a single endpoint measurement obscures these distinct mechanisms and limits the interpretability of stabilization strategies.

The present study addresses these gaps by conceptualizing foamed CLSM as a coupled process–material system. Rather than modifying composition alone, the investigation systematically varies mixing technology and rotational speed to quantify the influence of shear history. Surfactant dosage, FA replacement, and short coconut fiber incorporation are introduced as complementary mechanisms acting at the interfacial, rheological, and structural levels, respectively. By combining time-resolved volumetric monitoring with mechanical and physical characterization, the study seeks to clarify the relative dominance of process control versus material modification in governing early-age stability. Through this integrated framework, the work advances the understanding of volumetric stability beyond conventional density–strength correlations and provides a reproducible methodology for optimizing foamed CLSM in soft-ground applications. Unlike prior studies that treat foam stability primarily as a compositional or admixture-driven phenomenon, the present study explicitly isolates mixing sequence and shear regime as independent design variables and quantifies their interaction with interfacial, rheological, and structural stabilization mechanisms. By decoupling process-induced volumetric instability from material-induced volumetric instability, this work introduces a mechanistic hierarchy for early-age volumetric control, which has not been systematically established in CLSM systems incorporating dredged soil.

2. Materials and methods

2.1. Materials

All constituents were selected to reflect materials readily available in Ho Chi Minh City, Vietnam, thereby ensuring that the experimental findings remain transferable to typical urban infrastructure practice in the region. The mixtures were prepared using PCB40 cement, river sand, dredged soil, FA, short coconut fibers, a protein-based foaming agent, a non-ionic surfactant, and potable mixing water. PCB40 cement conforming to TCVN 6260:2020 was used as the primary binder. The cement satisfied the fineness requirement of at least 85% passing the 90 μm sieve in accordance with TCVN 4030:2003, and met the performance indices specified for 28-day compressive strength (≥ 40 MPa), initial setting time (≥ 45 min), and final setting time (≤ 375 min) following TCVN 6017:2015. River sand sourced locally complied with TCVN 7570:2006. Its fineness modulus fell within 2.0–2.6, the fines fraction below 0.075 mm was not greater than 5%, and the specific gravity was approximately 2.65 g/cm³. Dredged soil collected from canal-clearing operations represented a fine-grained material stream relevant to regional maintenance and excavation activities. Based on combined sieve and hydrometer analysis, the soil contained more than 50% fines. To reduce variability introduced by in-situ moisture, the soil was air-dried and screened prior to mixing. FA from the Pha Lai power plant was employed as a partial cement replacement. The combined $SiO_2 + Al_2O_3 + Fe_2O_3$ content was 85.6%, and the loss on ignition was 4.5%, satisfying the requirements of TCVN 10302:2014. Replacement levels between 10% and 40% were investigated to capture both the beneficial range (through packing and rheology) and the region where reduced cement content may affect early skeleton formation. Short-cut coconut fibers were incorporated to provide discrete reinforcement and potential early-age micro-locking within the evolving porous framework. The fibers had an approximate length of 2 mm and a diameter of 100–250 μm, and were dosed within 0.05–0.40% (consistent with the dosage convention adopted in the manuscript). Preformed foam was generated from a protein-based foaming agent. The produced foam exhibited a bulk density of 55–95 kg/m³, bubble diameters in the range of 100–400 μm, and water retention of at least 85%. Foam contents between 10% and 30% by volume were used to adjust the target density and void structure. A non-ionic surfactant, with surface tension of 30–35 mN/m and density of 1.00–1.05 g/cm³, was added at 0.05–0.30% of the foaming solution to enhance bubble-film stability during mixing and setting. The mixing water met the requirements of TCVN 4506:2012. The water had a pH of 6.5–7.5, chloride content not exceeding 500 mg/L, and sulfate content not exceeding 300 mg/L, minimizing the risk of uncontrolled setting effects and ensuring comparability among batches.

2.2. Aggregate analysis

Particle-size distribution results indicate a pronounced but complementary gradation contrast among the constituents, which is essential for understanding both fresh-state stability and the subsequent formation of a load-bearing skeleton. River sand served as the primary granular framework, with more than 95% of particles larger than 0.14 mm. In contrast, dredged soil exhibited typical fine-grained characteristics, with 68% passing the 0.075 mm sieve. This disparity supports a packing mechanism in which soil fines can occupy intergranular voids between sand particles, thereby increasing overall packing density and improving cohesion of the fresh matrix, which is particularly relevant for resisting drainage and bubble migration in foamed systems. For the binder fraction, PCB40 cement showed the highest fineness, with 92% passing the 45 μm sieve, which supports rapid early hydration and early bonding development. FA exhibited a slightly coarser distribution, with 82% passing 45 μm, functioning both as a fine filler and as a rheology modifier. Its spherical morphology is expected to contribute to workability through a ball-bearing effect while also improving micro-filling within the paste. All gradation measurements were conducted in accordance with TCVN 7570:2006, and the corresponding results are presented in Fig. 1.

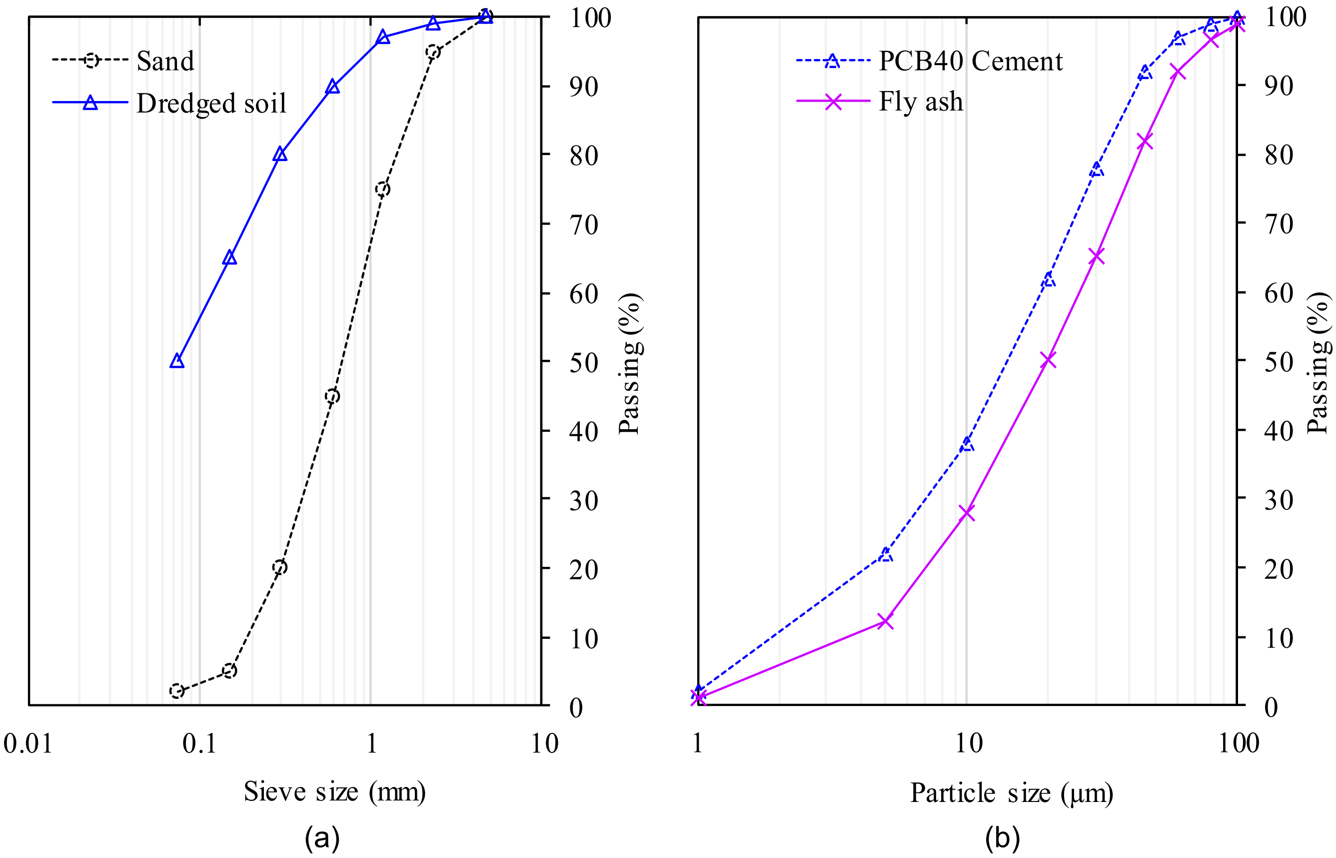

Fig. 1. Sieve comparison between (a) fine aggregate; (b) cement and FA

2.3. Mix design

To ensure consistency and allow meaningful attribution of observed responses to single factors, the experimental program was organized using a structured three-layer design logic. A fixed baseline mixture was first established. Standardized mixing procedures were then defined such that the only differences among mixing methods stem from the sequencing of water and foam introduction rather than uncontrolled handling. Finally, an experimental matrix was constructed using a design principle in which each group isolates one primary variable, so that each conclusion can be directly attributed to a single intended modification before evaluating synergistic effects in the combined configuration.

2.3.1. Fixed baseline mixture

A common baseline mixture (Table 1) was

adopted as the reference for all experimental groups and was kept unchanged throughout the program. Fixing the baseline is critical for isolating the effects of foam content, mixing procedure, surfactant dosage, FA replacement, and coconut fiber content on volumetric stability, flowability, and setting-stage behavior. By preventing drift in the underlying material proportions, the baseline-based design ensures that differences in performance can be interpreted mechanistically rather than being confounded by changes in paste volume, water content, or aggregate fraction.

Table 1. Baseline mixture for 1 m^3 of foamed CLSM

Component	Symbol	Unit	Design value
Dredged soil	D	kg/m^3	450
Sand	C	kg/m^3	450
PCB40 cement	CM	kg/m^3	150
Mixing water	W	kg/m^3 (≈ L/m^3)	180

Table 2. Mixing procedures

Code	Mixing Method	Stage B1	Stage B2	Stage B3
K	Dry mixing	Dry mix (Soil + Sand + Cement)	100% Water + Foam	–
U1	Wet mixing 1	Dry mix	100% Water	Foam
U2	Wet mixing 2	Dry mix	50% Water	50% Water + Foam

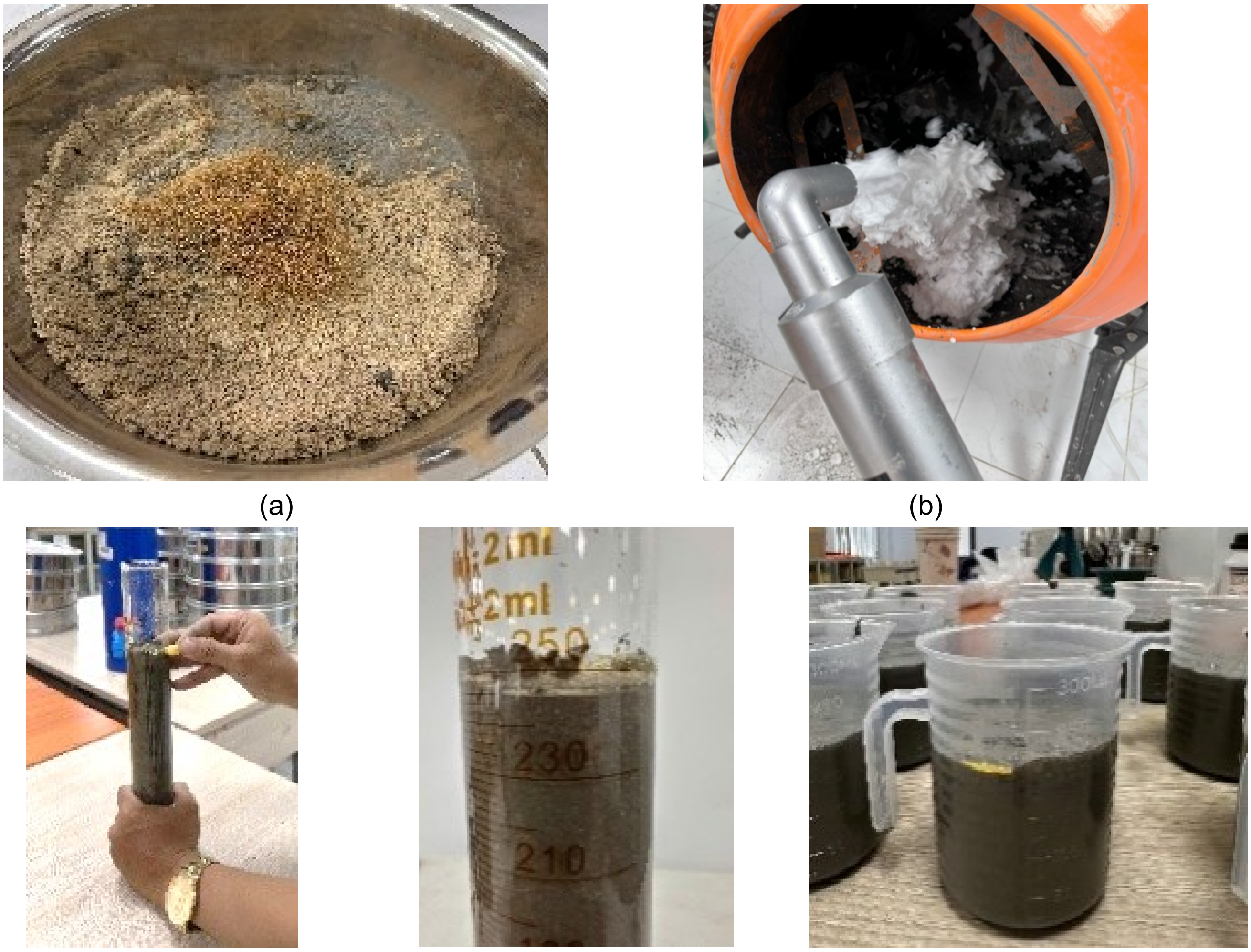

(a) (b)

(c)

Fig. 2. (a) mixture composition; (b) casting foam; (c) volumetric loss test; (d) flowability test; (e) UCS test

(d)

(e)

Fig. 2. (continued)

2.3.2. Standardized mixing procedures

Three mixing methods (K, U1, and U2) were defined and standardized through the same three-stage structure (B1–B3) summarized in Table 2. In all cases, stage B1 consisted of dry mixing of dredged soil, sand, and cement to ensure uniform dispersion of solids before any liquid phase was introduced. The methods then diverged only in the sequencing of water, foam, and admixture addition, thereby allowing the effect of mixing history to be quantified.

In method K, the full water content and foam were introduced together in stage B2. This configuration exposes bubble films to shear while the matrix is still relatively dilute, which can promote rupture and coalescence. In method U1, the full water content was added in stage B2 to form a slurry first, and foam was introduced afterward in stage B3. This sequencing generally reduces direct bubble exposure during the initial wetting and dispersion of solids. In method U2, the water was split into two equal portions: 50% was added in stage B2 to build a more cohesive matrix prior to foaming, and the remaining 50% was introduced simultaneously with foam in stage B3. This staged-water concept is intended to increase early cohesiveness and yield stress at the moment of foam incorporation, improving mechanical shielding of bubbles during mixing while still allowing final workability adjustment. These standardized procedures are designed so that differences in volumetric loss and workability originate from mixing sequence and the associated shear environment, rather than from inconsistent batch handling. Fig. 2 illustrates key steps and test setups supporting this standardization.

2.3.3. Experimental matrix

The experimental program (Table 3) was constructed following a controlled-variable logic in which each group targets one primary factor while holding all other conditions constant. In the first group, foam content was varied between 10% and 30% in a preliminary foam-content trial to establish the baseline sensitivity of volumetric loss to air volume fraction and to identify practical ranges for subsequent investigations. In the second group, mixing method (K/U1/U2) and mixer speed (30–60–90–120 rpm) were varied while foam content was fixed at representative levels (20–25%) to assess sensitivity to shear energy and foam-introduction sequence.

After establishing U2 at 60 rpm as the reference process condition, subsequent groups isolated the contribution of individual material modifications under fixed conditions (foam content 25%, U2 at 60 rpm). Surfactant dosage was examined from 0.05% to 0.30% of the foaming solution, FA replacement was varied from 0% to 40% by mass of cement, and coconut fiber content (2 mm) was varied from 0.05% to 0.40% by mass of solids. For consistency, S is reported throughout as a percentage of the foaming solution. The final group evaluated the combined solution using the optimal levels identified in the individual-material groups, and directly compared it against the control under identical process conditions. This sequence allows both independent effects and synergy to be assessed without ambiguity.

Table 3. Experimental matrix (based on the fixed baseline mixture)

Group	Objective	Variable	Levels	Fixed Conditions
G1	Effect of foam content	Foam (% vol.)	10, 15, 20, 25, 30	Preliminary trial; no FA, no fiber, S = 0
G2	Effect of mixing method and speed	Speed (rpm)	30, 60, 90, 120	Foam 20–25%, same water content, no FA, no fiber, S = 0
G3	Effect of surfactant dosage	S (% of foam solution)	0.05, 0.10, 0.15, 0.20, 0.30	Foam 25%, U2–60 rpm, no FA, no fiber
G4	Effect of FA replacement	FA (% cement replacement)	0, 10, 20, 25, 30, 40	Foam 25%, U2–60 rpm, S = 0, no fiber
G5	Effect of coconut fiber (2 mm)	Fiber (% of solid mass)	0.05, 0.10, 0.20, 0.30, 0.40	Foam 25%, U2–60 rpm, S = 0, no FA
G6	Combined solution	S + FA + Fiber	S*, FA*, Fiber*	Foam 25%, U2–60 rpm (compared to control)

*Note: * indicates the optimum level selected based on the minimum final volumetric loss (ΔV_Final) in the corresponding individual-material group: S = 0.15% of the foaming solution; FA = 25% cement replacement; and Fiber = 0.30% of solid mass.*

2.3.4. Mould preparation, casting, and curing

Compressive-strength specimens were cast in high-strength PVC cylindrical moulds with dimensions of 60 mm in diameter and 120 mm in height. Each mould featured a longitudinal split and external reinforcement to facilitate demoulding without damaging the specimen surface. Prior to casting, a thin layer of release oil was applied, and moulds were labeled to ensure traceability across groups and replicates.

For each mixture, three replicate specimens were prepared to control random variation. Although three replicates were adopted to maintain feasibility across the extensive parametric matrix, consistency of trends across independent variable groups was verified. The reported values represent mean measurements, and the observed response patterns were repeatable across batches. Future investigations incorporating larger sample sizes are recommended to enable formal statistical inference. Immediately after mixing, the fresh material was examined for spread, bleeding tendency, and fresh density to confirm batch uniformity prior to casting. Specimens were filled manually without vibration so that the natural behavior of the foamed matrix—particularly bubble stability under self-weight—was not artificially altered by compaction energy. After casting, specimens were covered and cured under laboratory conditions of 25 ± 2°C and relative humidity not less than 95%. After demoulding, samples were maintained under moist curing until the designated testing ages, and all specimens were cured under identical conditions to preserve comparability.

2.4. Testing methods

Fresh and hardened properties were evaluated using procedures aligned with established CLSM test standards. Volumetric loss was monitored using transparent graduated cylinders using a procedure adapted from ASTM C940, which tracks settlement and height change of flowable fills. Specimen height was recorded at casting and again after 5 min, at the initial setting time, and at the final setting time to quantify early-age volumetric stability (Fig. 2c). All measurements were performed using the same calibrated graduated cylinder, and each mixture was tested in three replicates. The reported values represent average measurements, and the observed trends were consistent across batches, confirming the repeatability of the method for comparative evaluation. Dry density was determined by oven-drying specimens at 105 ± 5°C to constant mass and calculating density using the measured dry mass and the cylindrical volume. Flow spread was assessed following ASTM D6103 (Fig. 2d) by measuring two perpendicular spread diameters and reporting the average value as the flow consistency index.

Setting time was determined using a Vicat apparatus following a procedure adapted from ASTM C191 under controlled curing conditions (27 ± 2°C and relative humidity ≥ 95%), allowing identification of both initial and final set for each mixture. The final setting time refers to the Vicat-determined final set; the corresponding ΔV measurements were taken at this final set. It should be emphasized that the reported volumetric loss prior to final set primarily reflects settlement and drainage-induced deformation rather than autogenous or drying shrinkage mechanisms, which occur after structural hardening. Water absorption was evaluated using a mass-difference approach commonly adopted for CLSM durability screening, by comparing oven-dry mass with saturated mass after immersion. Compressive strength was measured according to ASTM D4832 (Fig. 2e) using specimens tested at 7 and 28 days; the reported strength was obtained by dividing the peak load by the loading area.

3. Results and discussion

3.1. Baseline influence of foam content on volumetric loss

The baseline evaluation clearly demonstrates that foam content is the primary intrinsic parameter governing geometric instability prior to process or material optimization. These values were obtained from a preliminary foam-content trial without FA, fiber, or surfactant. As shown in Fig. 3, ΔV increased sharply and nonlinearly as foam content rose from 10% to 30%.

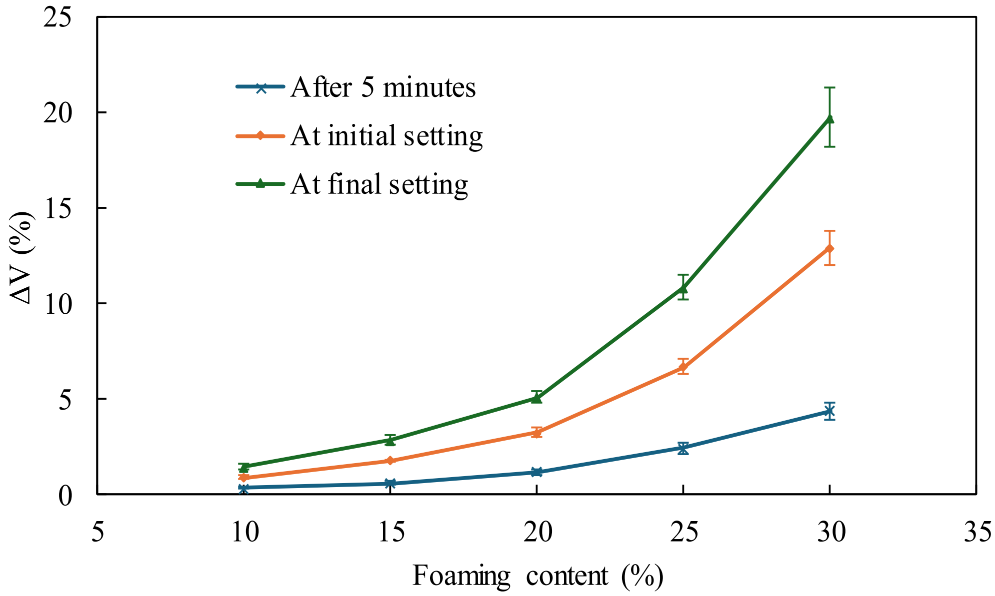

Fig. 3. Effect of foam content on volumetric loss at three evaluations

At 10% foam, ΔV_Final after setting was only 1.47%, indicating that the bubble network remained largely stable and that early skeletal formation effectively restrained post-setting deformation. However, at 20% foam, ΔV_Final increased to 5.12%, representing more than a threefold increase. Further increase to 25% foam resulted in ΔV_Final of 10.83%, while at 30% foam the value approached 19.8%, indicating severe structural volumetric instability during the setting period. The trend was consistent across all three monitoring stages (5 minutes, initial set, and final set), suggesting that both instantaneous bubble rupture during mixing and progressive drainage-induced volumetric instability during setting intensified as air fraction increased. The nonlinearity of the response is critical. The jump from 25% to 30% foam nearly doubled ΔV_Final, indicating that a threshold behavior exists once the paste phase becomes insufficient to maintain inter-bubble separation. This abrupt escalation indicates a transition from isolated bubble dispersion to interconnected gas-phase dominance, where the liquid film network becomes insufficient to sustain capillary equilibrium within the Plateau borders. Such threshold behavior suggests that beyond a critical gas volume fraction, volumetric instability becomes structurally inevitable regardless of minor compositional adjustments. This behavior aligns with established foam mechanics principles, where increased gas volume fraction reduces liquid film thickness and increases capillary pressure gradients within Plateau borders. Hashim and Tantray [4] reported similar volumetric instability escalation when bubble films become excessively thin under high air contents. The present data confirm that even in CLSM systems containing soil fines and FA, geometric instability is primarily driven by air fraction once a critical pore connectivity threshold is exceeded.

Importantly, the separation between the curves at 5 minutes and at the final set widens significantly at 25–30% foam. This indicates that volumetric instability is not limited to immediate shear damage but continues during the setting transition, where insufficient early skeleton formation fails to lock the pore structure. This observation justifies subsequent investigation of mixing sequence and rheological stabilization strategies.

3.2. Influence of mixing techniques

The effect of mixing technique under controlled foam contents (20% and 25%) reveals that process variables dominate geometric stability once air fraction is fixed. Fig. 4 shows that ΔV_Final increases with mixing speed for all three techniques, but the magnitude of sensitivity differs markedly.

Under the K method (dry mixing), ΔV_Final for 20% foam increased from 6.83% at 30 rpm to 13.87% at 120 rpm. At 25% foam, the increase was even more pronounced, rising from 10.83% to 19.82%. The near-linear increase with rotational speed suggests direct shear-induced bubble rupture prior to structural stabilization. Furthermore, the increasing separation between 5-minute and final-set curves indicates that early shear damage propagates into late-stage volumetric instability, consistent with cumulative coalescence effects.

In contrast, the U1 method significantly reduced sensitivity to shear. At 25% foam, ΔV_Final increased from 8.63% (30 rpm) to 12.36% (120 rpm), corresponding to reductions of approximately 15–38% relative to K under identical conditions. At the intermediate speed of 60 rpm, ΔV_Final was 7.41%, compared with 12.68% for K. This confirms that delaying foam introduction until after slurry formation mitigates direct shear exposure. The most pronounced stabilization occurred in U2. For 20% foam at 60 rpm, ΔV_Final was only 3.96%, representing approximately 55% reduction relative to K (8.62%) and 20% relative to U1 (4.93%).

At 25% foam and 60 rpm, ΔV_Final was 5.91%, compared with 7.41% (U1) and 12.68% (K). Moreover, the vertical spacing among 5-minute, initial-set, and final-set curves was minimal in U2 at 30–60 rpm, indicating that geometric stability was largely preserved throughout the setting period. The superior performance of U2 can be interpreted through rheological evolution. In particular, the staged-water approach enables partial development of matrix cohesion prior to foam incorporation, resulting in a higher effective yield stress and viscosity at the moment of bubble introduction. This rheological state provides mechanical shielding for bubble films, reducing their exposure to shear-induced rupture and limiting bubble coalescence during mixing. In contrast, when foam is introduced into a less cohesive matrix, the bubble network is more susceptible to deformation and collapse under the same shear conditions. Therefore, the improved stability observed in U2 reflects a combined effect of controlled sequencing and rheology-mediated protection of the pore structure. Cho et al. [6] demonstrated that foam stability in cementitious systems is strongly governed by shear energy and matrix viscosity during mixing. The present data quantitatively validate this mechanism in CLSM systems containing dredged soil.

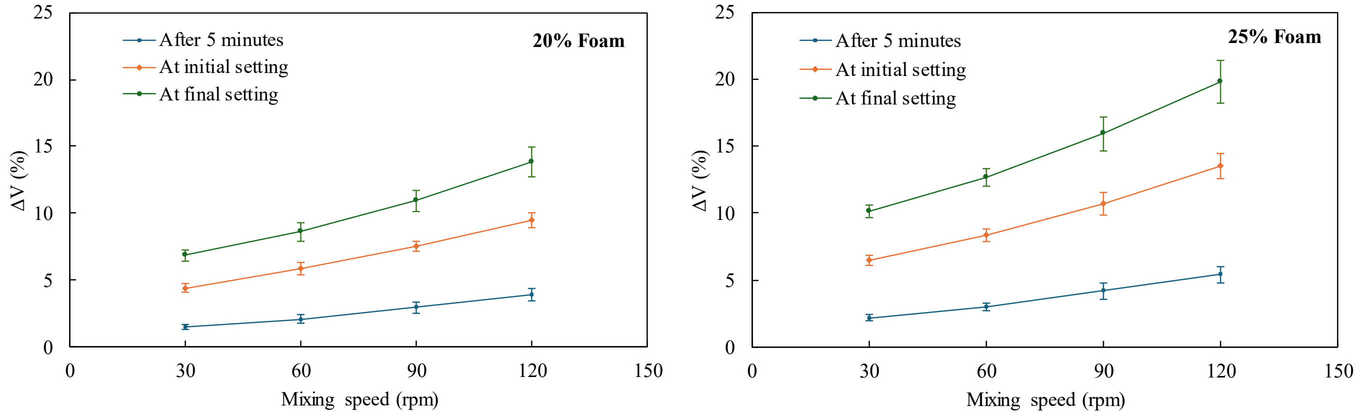

(a) K method (Full dry)

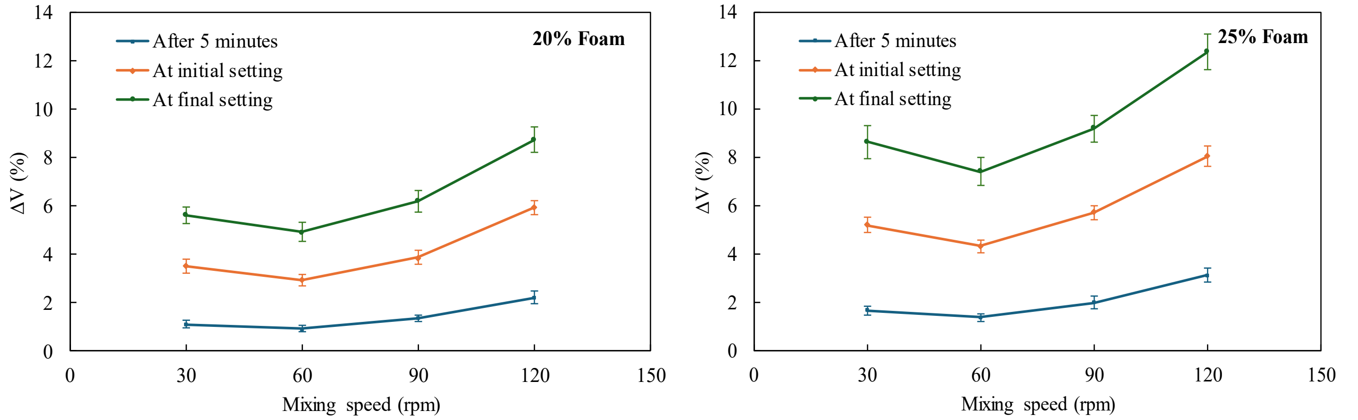

(b) U1 method (Full wet)

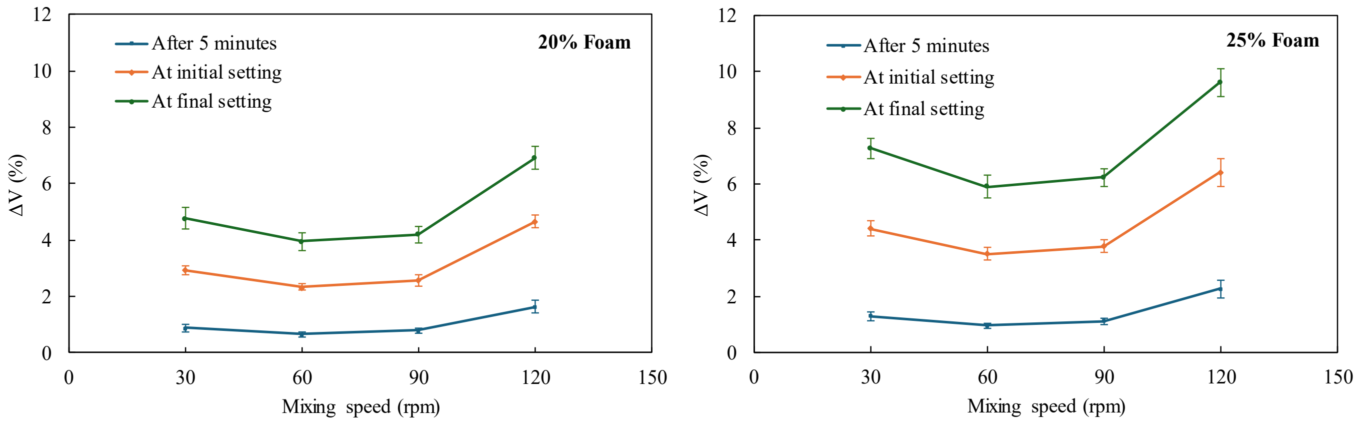

(c) U2 method (Half wet method)

Fig. 4. Effect of mixing sequence (K, U1, U2) and rotational speed on time-resolved volumetric loss at 20% and 25% foam

The combined influence of mixing speed and sequence reveals an optimal regime at 60 rpm. Quantitatively, under 25% foam, the reduction from 12.68% (K–60 rpm) to 5.91% (U2–60 rpm) corresponds to approximately 53–55% improvement achieved solely through process modification without altering material composition. This magnitude exceeds the improvement obtained from any individual material intervention, reinforcing the process-dominant nature of early-age stability. At 30 rpm, dispersion may be insufficient, leading to non-uniform bubble distribution. At 120 rpm, shear energy exceeds bubble film resistance, causing rupture even under U2. Thus, volumetric stability is not solely a function of composition but of controlled shear history.

3.3. Influence of surfactant dosage on volumetric loss of foamed CLSM

Fig. 5 shows that surfactant dosage exerts a nonlinear influence on ΔV across all three evaluation stages. Under the optimized U2–60 condition with 25% foam, the control mixture (C0-best) exhibited ΔV_Final of 5.91% and ΔV at the initial setting of 3.52%.

At 0.05% dosage, ΔV_Final decreased modestly to 5.22%, while ΔV at the initial set decreased to 3.08%. The small magnitude of reduction indicates that partial surface-tension modification occurred but was insufficient to significantly reinforce bubble films. At this stage, stabilization is limited by incomplete surface coverage and weak interfacial elasticity. A clearer improvement appeared at 0.10%, where ΔV_Final dropped to 4.63%, and ΔV at the initial set and 5 minutes decreased to 2.74% and 0.66%, respectively. This simultaneous reduction across early and late stages suggests enhanced resistance to both immediate rupture and drainage-induced volumetric instability.

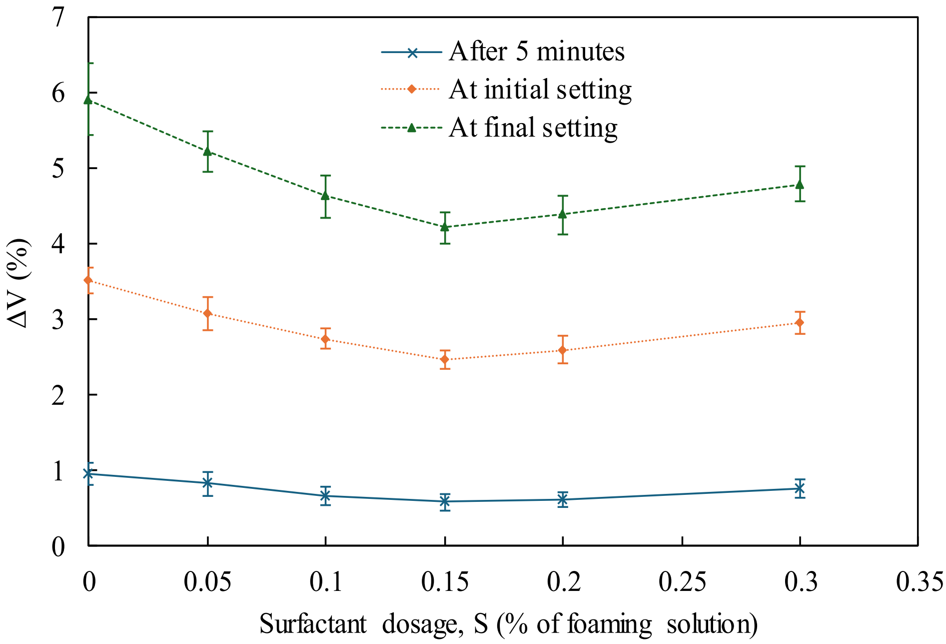

Fig. 5. Effect of surfactant dosage (S) on time-resolved volumetric loss under U2–60 rpm and 25% foam

The optimum occurred at 0.15%, where ΔV_Final reached 4.21%, representing a 28.8% reduction relative to C0-best. ΔV at the initial set decreased to 2.46%, and at 5 minutes to 0.58%. The balanced reduction at all stages implies that bubble films achieved sufficient elasticity and uniform dispersion within the matrix. Hashim and Tantray [4] reported that protein-based foaming systems exhibit an optimal surfactant concentration beyond which film elasticity no longer increases proportionally, and excessive adsorption may alter rheological interactions. The present results align closely with that mechanism.

At 0.20%, ΔV_Final increased slightly to

4.38%, and at 0.30% it further increased to 4.79%. Although still lower than the control, the upward trend indicates overdosing. Excess surfactant may produce overly stable microbubbles that resist coalescence locally but promote clustering and uneven dispersion, leading to macro-instability. Cho et al. [6] observed similar deterioration under overdosing in printable foamed concrete. The data therefore confirm that chemical stabilization must be carefully balanced and cannot substitute for process control.

3.4. Influence of FA replacement on the volumetric loss of foamed CLSM

Fig. 6 shows that FA replacement modifies ΔV through a combination of rheological enhancement and hydration kinetics. Compared with the 0% FA control (ΔV_Final = 5.91%), increasing FA to 10% reduced ΔV_Final to 5.52%. At 20%, ΔV_Final decreased further to 4.96%, and at 25% reached a minimum of 4.56%. ΔV at the initial set followed the same trend, decreasing from 3.52% (0%) to 3.02% (20%) and 2.83% (25%). The progressive reduction up to 25% FA suggests enhanced water retention and paste cohesion. FA particles improve packing density and increase paste viscosity without dramatically reducing workability. Han et al. [9] reported similar improvements in flowable CLSM with moderate FA incorporation, attributing stability gains to reduced bleeding and improved micro-filling.

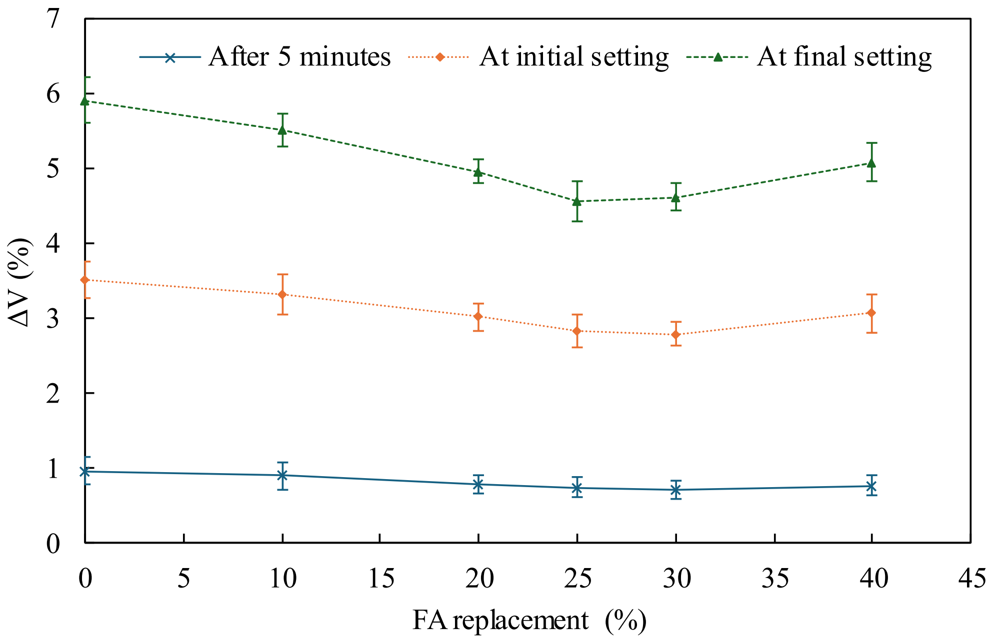

Fig. 6. Effect of FA replacement on time-resolved volumetric loss under U2–60 rpm and 25% foam

At 30% FA, ΔV_Final increased slightly to 4.62%, and at 40% rose to 5.08%, with ΔV at the initial set increasing to 3.06%. This reversal reflects reduced cement content and delayed early hydration, which weakens early skeleton formation. Ho et al. [14] demonstrated that high-volume FA systems exhibit slower strength gain and reduced early stiffness. In a highly porous foamed matrix, delayed structural locking allows continued bubble migration during setting. Thus, FA acts primarily through rheological stabilization up to an optimum range (~25%) but compromises early framework formation beyond that threshold.

3.5. Influence of coconut fiber content on the volumetric loss of foamed CLSM

Fig. 7 illustrates that fiber influence differs from surfactant and FA. The effect at 5 minutes is minimal, while reductions are more pronounced at the initial and final set. At 0.1% fiber, ΔV_Final decreased slightly from 5.91% to 5.21%, and ΔV at the initial set from 3.52% to 3.18%. At 0.20%, ΔV_Final decreased to 5.06%, representing approximately 14% reduction relative to the control. However, unlike surfactant or FA, fiber did not produce dramatic early-stage stabilization. The mechanism is primarily mechanical rather than interfacial. Du et al. [5] demonstrated that short fibers form micro-bridging networks that restrain deformation and improve bubble stability in foamed matrices. The present data indicate that fiber reinforcement becomes effective once a semi-continuous solid phase develops, explaining why improvements are more evident at initial and final set than at 5 minutes. At 0.30%, ΔV_Final reached 4.89%, but at 0.40% increased to 5.64%, with ΔV at the initial set rising to 3.46%. This confirms that excessive fiber dosage leads to agglomeration and heterogeneity, disrupting bubble dispersion and counteracting stabilization. The lowest measured final-set volumetric loss was obtained at 0.30% fiber, whereas the maximum 28-day compressive strength occurred at 0.20%. Therefore, the preferred fiber dosage depends on whether volumetric stability or mechanical performance is adopted as the primary optimization criterion.

3.6. Effectiveness of individual and combined material modifications under different mixing technologies

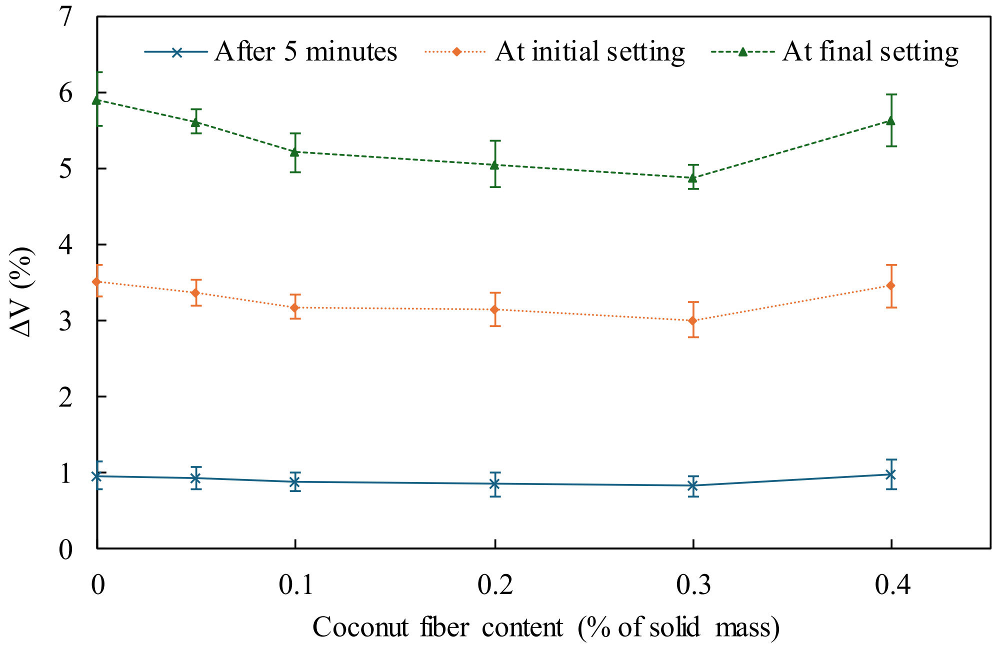

Fig. 7. Effect of 2 mm coconut fiber content on time-resolved volumetric loss under U2–60 rpm and 25% foam

Fig. 8 clearly shows that the magnitude of material improvement depends on the underlying mixing condition. Under U2–60 with 25% foam, S-best reduced ΔV_Final from 5.91% to 4.21% (28.8% reduction), F-best reduced it to 4.56% (22.8%), and C-best to 4.89% (17.3%). The ranking S > FA > fiber reflects the dominance of interfacial stabilization once shear is controlled. The combined SFC-best configuration reduced ΔV_Final to 2.78%, which is substantially lower than any individual modification and indicates multi-scale interaction among interfacial reinforcement, rheological cohesion, and structural micro-bridging. While not strictly additive in a linear sense, the cumulative reduction demonstrates cooperative stabilization across scales. Under the worst-case K–120 condition with 25% foam, ΔV_Final of C0-worst reached 19.82%. Even with material modification, reductions were limited: 15.96% (S-worst), 16.71% (F-worst), and 17.52% (C-worst). Monkman et al. [10] showed that excessive shear can irreversibly damage foam structure despite rheology modification. The present data confirm that process control is a prerequisite for material-based stabilization. Overall, the three material strategies operate through distinct but complementary mechanisms. Surfactant primarily stabilizes the air–liquid interface by enhancing bubble film elasticity and resistance to coalescence. FA contributes to rheological cohesion and reduced drainage through improved particle packing and paste viscosity. Coconut fiber provides structural reinforcement during the setting transition by forming a micro-bridging network within the evolving skeleton. The combined SFC configuration integrates these interfacial, rheological, and structural effects, resulting in multi-scale stabilization of the foamed matrix.

3.7. Relationship between post-setting volume loss and 28-day compressive strength

Fig. 9a presents the relationship between post-setting volumetric loss (ΔV_Final) and 28-day compressive strength under the U2–60 rpm condition with 25% foam. All reported values represent the mean of three replicates. Although a general tendency exists whereby improved volumetric stability corresponds to improved mechanical performance, the relationship is not directly proportional. This indicates that early geometric stability and long-term load-bearing capacity are governed by overlapping but distinct mechanisms. The control mixture (C0-best) exhibited a ΔV_Final of 5.91% and a 28-day compressive strength of 1.42 MPa. When surfactant was incorporated at the optimal dosage (S-best), ΔV_Final decreased markedly to 4.21%, yet the compressive strength decreased slightly to 1.31 MPa. This divergence confirms that interfacial stabilization alone does not enhance structural densification. The surfactant reinforces bubble membranes and improves dispersion uniformity, but it does not contribute to hydration bonding or solid-phase continuity. Similar decoupling between pore stability and strength has been reported in lightweight foamed systems, where compressive performance depends more strongly on skeleton integrity than on volumetric preservation alone [1]. In contrast, the FA-modified mixture (F-best) achieved a ΔV_Final of 4.56% with a corresponding compressive strength of 1.5 MPa. The modest strength enhancement reflects the dual role of FA: improved rheological cohesion and reduced drainage in the fresh stage, combined with gradual pozzolanic contribution at later ages. However, in a highly porous foamed matrix with limited cement content, the pozzolanic effect at 28 days remains moderate. The 0.30% coconut fiber mixture (C-best), selected based on volumetric stability, showed a different coupling behavior. Although ΔV_Final was 4.89%, higher than that of S-best and F-best, the compressive strength increased significantly to 1.58 MPa. This confirms that fiber reinforcement enhances load transfer through micro-bridging and crack-arrest mechanisms within the porous skeleton, even when volumetric stability is not maximally optimized. The combined system (SFC-best) exhibited the most balanced response, reducing ΔV_Final to 2.78% while increasing compressive strength to 1.62 MPa. This simultaneous improvement indicates synergistic stabilization across interfacial, rheological, and structural levels. Fig. 9b further supports this interpretation: SFC-best achieved the highest dry density (1256 kg/m³) and the lowest water absorption (13.4%), confirming that enhanced early-age stability leads to a more homogeneous and less connected pore structure in the hardened state.

3.8. 28-day compressive strength results

The 28-day compressive strength results shown in Fig. 10 demonstrate distinct strengthening mechanisms for surfactant, FA, and coconut fiber modifications. For the surfactant series, compressive strength remained within a narrow range of 1.31–1.42 MPa across the dosage spectrum. The lowest strength (1.31 MPa) corresponded to the optimal ΔV reduction at 0.15% dosage. This slight reduction can be attributed to the lubricating effect of surfactant, which may reduce particle interlocking and local matrix stiffness. The relatively limited variation confirms that surfactant acts primarily at the air–liquid interface rather than enhancing the load-bearing skeleton. The FA series exhibited a modest but consistent increase in strength, reaching a maximum of 1.50 MPa at 25% replacement before declining at higher levels. The peak aligns with the optimal ΔV performance identified in Section 3.4. Moderate FA incorporation improves particle packing and hydration uniformity, contributing to skeleton densification. However, excessive replacement reduces effective clinker content, limiting early stiffness in the porous matrix. The coconut fiber series showed the most pronounced strengthening effect. Strength increased from 1.42 MPa (0%) to 1.62 MPa at 0.20% fiber dosage, then decreased slightly at 0.40% (1.49 MPa). The optimum corresponds to effective fiber dispersion and micro-bridging within the pore network. At higher contents, fiber agglomeration likely reduces uniformity and creates localized defects.

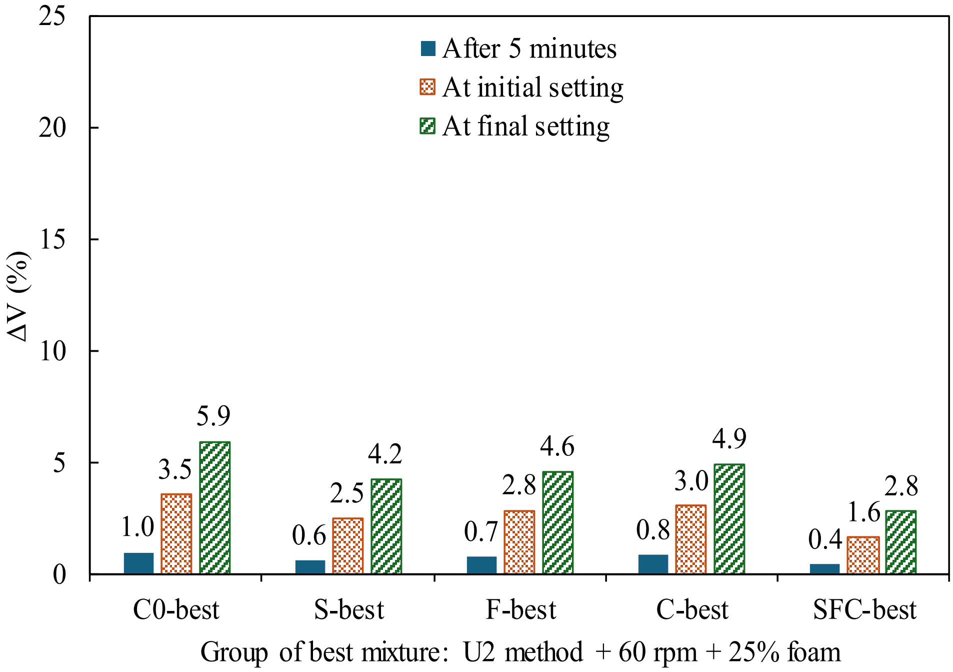

(a) Group of the best mixture

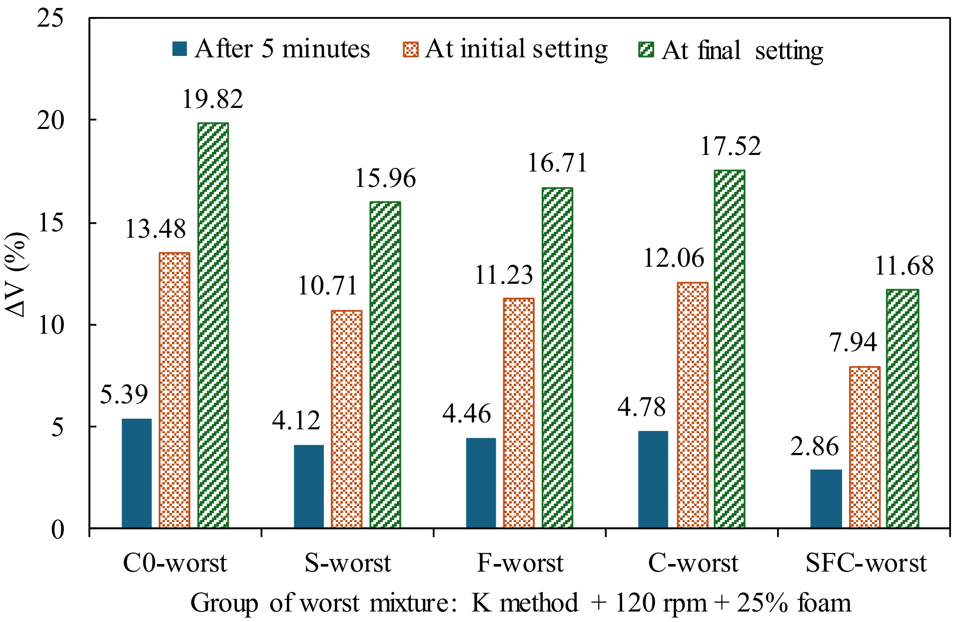

(b) Group of the worst mixture

Fig. 8. Comparative effectiveness of individual and combined stabilizers under best-case (U2–60) and worst-case (K–120) mixing regimes at 25% foam

(a)

(b)

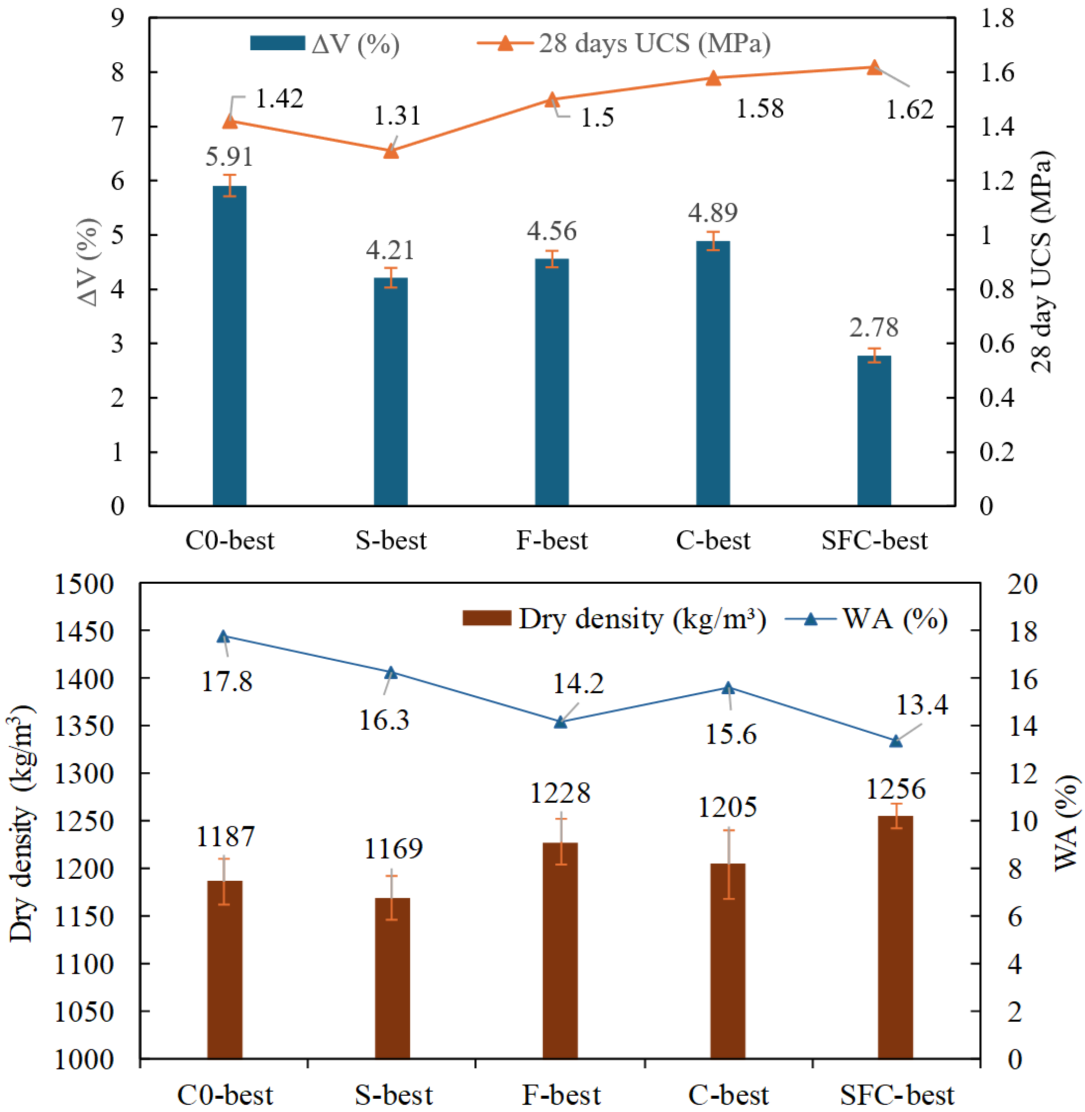

Fig. 9. (a) Relationship between final-stage volumetric loss and 28-day compressive strength under the U2–60 (25% foam) condition. (b) Variation of dry density and water absorption as influenced by material solutions

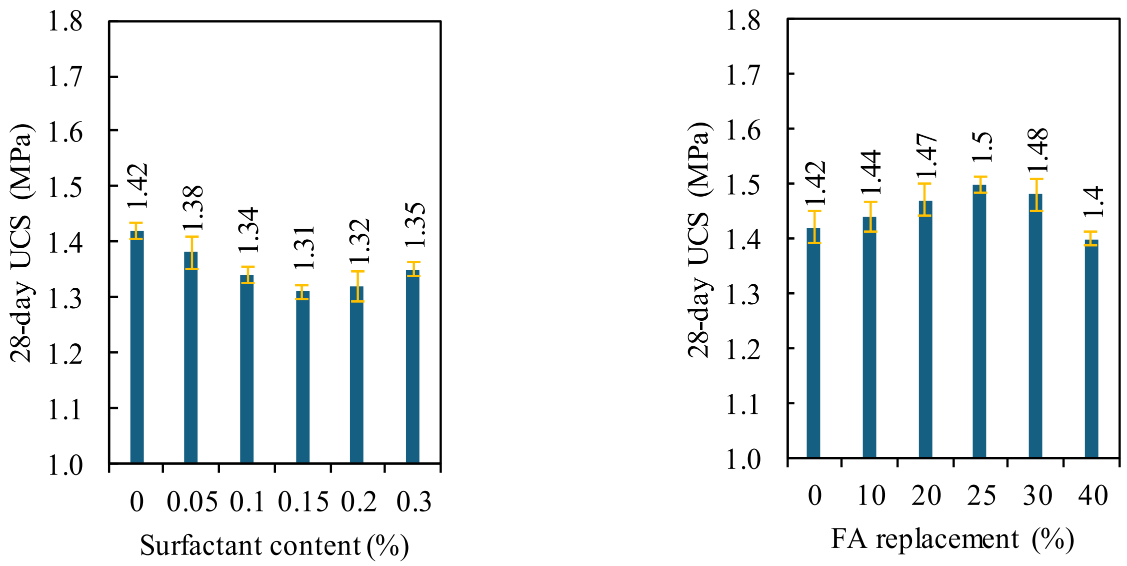

Fig. 10. 28-day UCS response to surfactant, FA, and coconut fiber dosage series

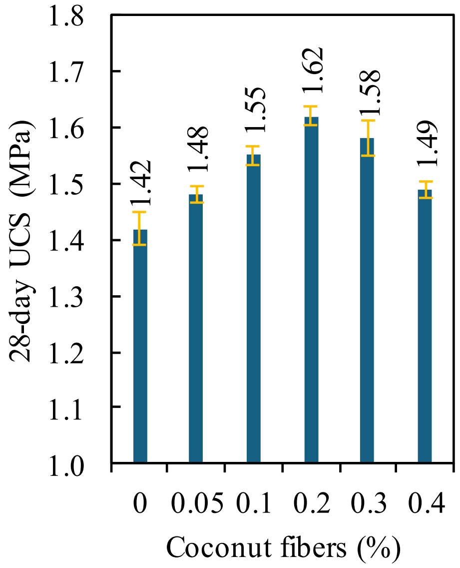

Fig. 10. (continued)

Overall, Fig. 10 confirms that surfactant contributes minimally to strength development, FA provides moderate matrix enhancement within an optimal range, and fiber reinforcement delivers the most significant improvement in load-bearing performance.

3.9. Qualitative relationship between post-setting volume loss and rheological behavior

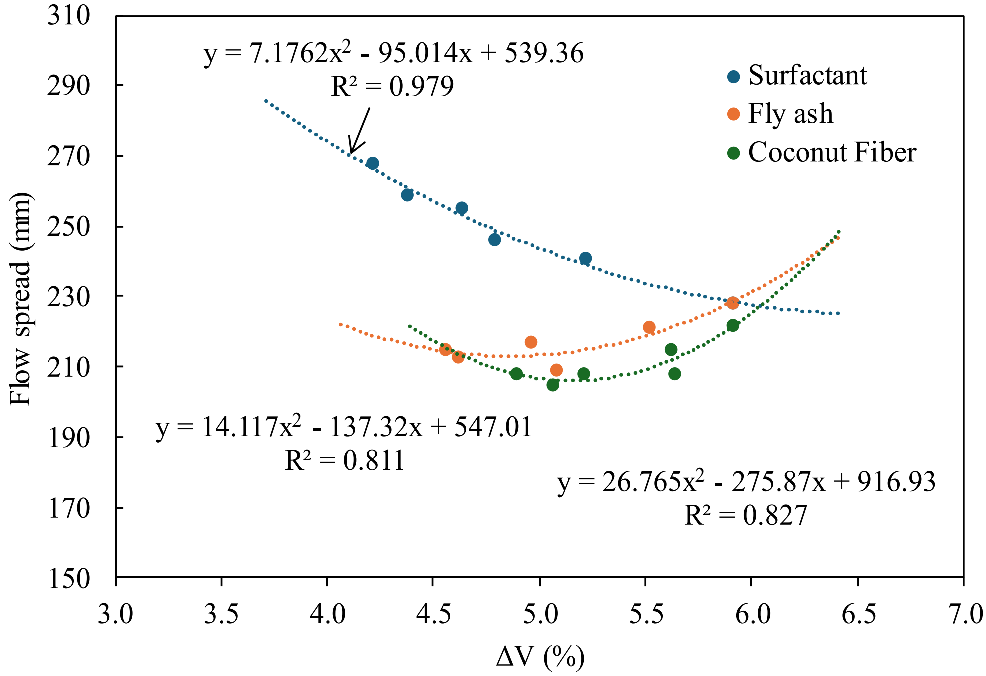

Fig. 11. Qualitative relationship between post-setting volumetric loss (ΔV_Final) and flowability across surfactant, FA, and coconut fiber series

In this study, flow spread is used as a practical proxy indicator of fresh-state deformability, rather than a full rheological characterization. Fig. 11 illustrates the qualitative relationship between ΔV_Final and fresh-state flow spread under identical mixing technology. The results indicate that volumetric stability and workability are not inherently contradictory; rather, their interaction depends on the stabilization mechanism. For the surfactant group, lower ΔV_Final values corresponded to increased spread diameter. At 0.15% dosage, ΔV_Final decreased to 4.21% while flowability reached 268 mm. This indicates that surfactant stabilizes bubble films without increasing bulk viscosity, enabling improved flow while preserving pore integrity. The stabilization mechanism is therefore interfacial rather than rheology-driven. For the FA and coconut fiber groups, the relationship is more complex. FA incorporation slightly reduced spread diameter while improving ΔV_Final, reflecting increased paste cohesion and reduced drainage. Fiber addition also reduced flowability due to mechanical interlocking and increased internal friction. In these cases, stabilization is partially associated with enhanced matrix resistance to deformation. It should be emphasized that Fig. 11 does not establish a predictive model. Instead, it provides mechanistic insight into how fresh-state rheological behavior interacts with early geometric stability. Quantitative modeling would require dedicated rheological parameters such as yield stress and plastic viscosity, which are beyond the scope of the present investigation.

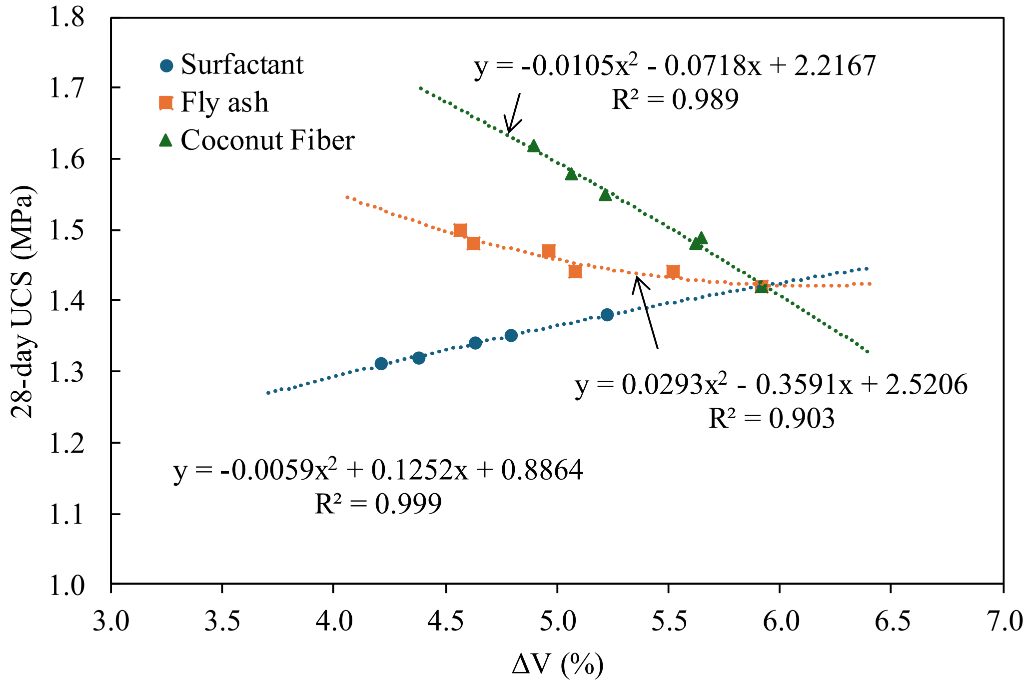

Fig. 12. Relationship between final-set volumetric loss and 28-day UCS

3.10. Relationship between post-setting volume loss and 28-day compressive strength across material groups

Fig. 12 presents the broader relationship between ΔV_Final and 28-day compressive strength across surfactant, FA, and coconut fiber groups. The data demonstrate that volumetric stability alone does not dictate compressive performance; instead, each material group follows a characteristic response pattern reflecting its stabilization mechanism. In the surfactant group, reductions in ΔV_Final are not accompanied by strength increases. In some cases, lower ΔV_Final corresponds to slightly reduced strength. This confirms that interfacial bubble stabilization improves geometric integrity but does not strengthen the cementitious skeleton. In the FA group, a moderate interaction zone is observed. Reductions in ΔV_Final correspond to slight strength improvements up to 25% replacement, beyond which strength decreases despite acceptable volumetric stability. This reflects the balance between rheological improvement and reduced clinker content. In the coconut fiber group, reductions in ΔV_Final within the mid-range are accompanied by strength enhancement. This pattern highlights the structural contribution of fiber bridging, which enhances load redistribution and crack resistance in the porous network. The fitted curves in Fig. 12 are intended to visualize within-series trends rather than to propose predictive models, given the limited number of dosage levels per material group. Fig. 12, therefore, reinforces a key conclusion of this study: early-age volumetric stabilization is a necessary but not sufficient condition for mechanical optimization. The highest performance is achieved when interfacial stabilization, rheological cohesion, and structural reinforcement are integrated within a controlled shear regime. The SFC-best mixture embodies this integrated mechanism, demonstrating that volumetric control and mechanical enhancement can be achieved simultaneously through hierarchical process–material design.

4. Conclusions

This study establishes a process-based framework for governing early-age volumetric stability in CLSM, incorporating dredged soil, integrating mixing sequence, shear intensity, and multi-scale material stabilization mechanisms.

The experimental results demonstrate that foam content fundamentally controls geometric sensitivity; however, volumetric instability escalates nonlinearly beyond approximately 25% foam, where ΔV increases sharply due to insufficient paste continuity and progressive bubble coalescence. At 30% foam, ΔV_Final approached 19.8%, confirming the existence of a stability threshold governed by air-phase connectivity.

Mixing sequence and shear regime were identified as the dominant stabilization factors. Among the evaluated techniques, the staged-water incorporation method (U2) at 60 rpm provided the most stable configuration, reducing ΔV_Final to 5.91% at 25% foam—approximately 55% lower than the dry-mix condition at comparable rotational speed. Excessive shear (120 rpm) led to irreversible bubble rupture, and material modifications were unable to fully compensate for this damage. These findings confirm that volumetric stability in CLSM is process-controlled during the fresh stage.

Material-level interventions acted as secondary stabilizers. Surfactant dosage of 0.15% yielded the most effective interfacial reinforcement, reducing ΔV_Final by 28.8% relative to the process-controlled baseline. FA replacement improved stability up to an optimum of approximately 25%, beyond which delayed early skeleton formation reduced effectiveness. Short coconut fiber at 0.20% enhanced structural integrity during the setting transition, contributing primarily to mechanical restraint rather than initial bubble protection.

The combined SFC configuration reduced ΔV_Final to 2.78% and increased 28-day compressive strength to 1.62 MPa, confirming synergistic interaction across interfacial, rheological, and structural scales. The inverse relationship between ΔV and compressive strength indicates that early-age geometric stability is a prerequisite for preserving homogeneous pore architecture and maintaining load-bearing capacity.

Overall, the study clarifies that early-age volumetric instability in foamed CLSM arises from cumulative shear damage and drainage-induced volumetric instability prior to structural locking. Effective stabilization requires hierarchical control: first, regulation of shear history through optimized mixing; second, enhancement of matrix cohesion and bubble-film elasticity; and third, mechanical reinforcement during skeleton formation. This framework provides a reproducible basis for designing lightweight CLSM systems suitable for soft-ground infrastructure while utilizing locally available dredged soil.

From a practical perspective, the findings indicate that controlling mixing sequence and shear conditions provides a reliable and scalable approach for improving early-age stability in foamed CLSM, while material modifications can be used as supplementary adjustments depending on project requirements. This process–material framework offers a practical basis for field implementation in soft-ground backfilling, where consistent mixing control can be achieved using standard construction equipment.

Acknowledgment

This research is supported by Nguyen Tat Thanh University and Can Tho University.

Declaration of Generative AI

During the preparation of this work, the authors do not use Generative AI and AI-assisted technologies tools in order to generate the content of the manuscript.

References

[1] S.H. Wong, P.N. Shek, A. Saggaff, M.M. Tahir, Y.H. Lee. (2019). Compressive strength prediction of lightweight foamed concrete with various densities. *IOP Conference Series: Materials Science and Engineering*, 620, 012043. DOI 10.1088/1757-899X/620/1/012043

[2] J.-M. Kim, J.-Y. Jeong. (2012). Influence of foaming agents on the properties of foamed concretes having various densities. *Journal of the Korea Institute of Building Construction,* 12(1), 22–30. http://dx.doi.org/10.5345/JKIBC.2012.12.1.022

[3] X. Shi, Y. Zhang, H. Hu, E.N. Arachchi, X. Cen, W. Li, Q. Wang. (2025). Role of red mud as a foam stabilizer in geopolymer foam concrete: Enhancing stability, rheology, and mechanical performance. *Journal of Building Engineering,* 105, 112446. https://doi.org/10.1016/j.jobe.2025.112446

[4] M. Hashim, M. Tantray. (2021). Comparative study on the performance of protein and synthetic-based foaming agents used in foamed concrete. *Case Studies in Construction Materials*, 14, e00524. https://doi.org/10.1016/j.cscm.2021.e00524

[5] Z. Du, P. Liu, P. Wang, M. Gao, Y. Shi, M. Sun, S. Jiang, L. Cui, S. Lv. (2025). Enhancing foam stability and performance in foam concrete using para-aramid nanofiber. *Journal of Building Engineering*, 103, 112139. https://doi.org/10.1016/j.jobe.2025.112139

[6] S. Cho, A. van Rooyen, E. Kearsley, G. van Zijl. (2022). Foam stability of 3D printable foamed concrete. *Journal of Building Engineering*, 47, 103884. https://doi.org/10.1016/j.jobe.2021.103884

[7] C. Honglei, J. Zuquan, Z. Tiejun, W. Benzhen, L. Zhe, L. Jian. (2020). Capillary suction induced water absorption and chloride transport in non-saturated concrete: The influence of humidity, mineral admixtures and sulfate ions. *Construction and Building Materials*, 236, 117581. https://doi.org/10.1016/j.conbuildmat.2019.117581

[8] J. Kanadasan, H.A. Razak, V. Subramaniam. (2018). Properties of high flowable mortar containing high volume palm oil clinker (POC) fine for eco-friendly construction. *Journal of Cleaner Production*, 170, 1244–1259. https://doi.org/10.1016/j.jclepro.2017.09.068

[9] J. Han, Y. Jo, Y. Kim, B. Kim. (2023). Development of high-performance fly-ash-based controlled low-strength materials for backfilling in Metropolitan Cities. *Applied Sciences*, 13(16), 9377. https://doi.org/10.3390/app13169377

[10] S. Monkman, S.D. Hwang, K. Khayat. (2024). Rheology modification of flowable mortar with CO_2. *Cement and Concrete Composites*, 151, 105584. https://doi.org/10.1016/j.cemconcomp.2024.105584

[11] W. Shen, Z. Zhang, J. Li, Z. Li, Z. Wang, L. Cao, G. Rong, M. Wu, D. Zhao, Z. Zhao. (2022). Experimental investigation on the high-volume fly ash ecological self-compacting concrete. *Journal of Building Engineering*, 60, 105163. https://doi.org/10.1016/j.jobe.2022.105163

[12] Z. Wan, T. He, N. Chang, X. Ma, H. Qiu, R. Yang, Q. Qu, et al., (2024). Effect of super absorbent polymer (SAP) on volume stability and application performance of cement mortar with accelerator. *Journal of Building Engineering*, 82, 108238. https://doi.org/10.1016/j.jobe.2023.108238

[13] V.L. Tang, Đ.T. Vo, K.D. Vu, B.B. Nguyen. (2023). Possibility to manufacture lightweight concrete from aluminum powder, mineral additives, and binders without cement. *The Proceedings of the International Conference - Celebrating 60 Years of IBST 2023, pp. 319–325*. (in Vietnamese).

[14] L.S. Ho, L.V. Quang, D.-T.V. Pham, T.-P. Huynh. (2025). Strength development and microstructural characterization of eco-cement paste with high-volume fly ash. *Results in Engineering*, 26, 105013. https://doi.org/10.1016/j.rineng.2025.105013

[15] A.T. Le, N.T. Nguyen, T.K. Nguyen. (2021). Study on geopolymer concrete based fly ash and slag of thermal plant and foam agent H_2O_2. *Journal of Materials and Construction*, 11(4), 6–12. (in Vietnamese). https://doi.org/10.54772/jomc.04.2021.145